Applied Catalysis B: Environmental 121–122 (2012) 65–74

Contents lists available at SciVerse ScienceDirect

Applied Catalysis B: Environmental

journal homepage: www.elsevier.com/locate/apcatb

Highly efficient multifunctional dually-substituted perovskite catalysts $La_{1-x}K_xCo_{1-y}Cu_yO_{3-\delta}$ used for soot combustion, NO*x* storage and simultaneous NO*x*-soot removal

Zhaoqiang Li[a], Ming Meng[a,*], Yuqing Zha[a], Fangfang Dai[a], Tiandou Hu[b], Yaning Xie[b], Jing Zhang[b]

[a] Tianjin Key Laboratory of Applied Catalysis Science & Engineering, School of Chemical Engineering & Technology, Tianjin University, Tianjin 300072, PR China
[b] Beijing Synchrotron Radiation Facility, Institute of High Energy Physics, Chinese Academy of Sciences, Beijing 100049, PR China

ARTICLE INFO

Article history:
Received 3 February 2012
Received in revised form 15 March 2012
Accepted 25 March 2012
Available online 1 April 2012

Keywords:
Soot combustion
NO*x* reduction
Perovskite
Dual substitution
Mechanism

ABSTRACT

A series of K/Cu simultaneously substituted nanometric perovskite catalysts $La_{1-x}K_xCo_{1-y}Cu_yO_{3-\delta}$ ($x = 0$, 0.1; $y = 0$, 0.05, 0.1, 0.2, 0.3) were synthesized by citric acid complexation, which were employed for soot combustion, NO*x* storage and simultaneous NO*x*-soot removal. The physico-chemical properties of the catalysts were characterized by XRD, FT-IR, EXAFS, SEM, H_2-TPR, Soot-TPR, TG/DTA, XPS and *in situ* DRIFTS techniques. When K and Cu are simultaneously introduced into $LaCoO_3$, soot combustion is largely accelerated, decreasing the characteristic temperature (T_m) corresponding to the maximal soot combustion rate at least 80 °C; moreover, NO*x* reduction by soot is also remarkably facilitated. Among all the catalysts $La_{0.9}K_{0.1}Co_{0.9}Cu_{0.1}O_{3-\delta}$ shows the lowest T_m of 360 °C, the highest NO*x* storage capacity (NSC) of 284 μmol g^{-1} and the largest NO*x* reduction percentage of 32%; for soot combustion, it also exhibits the lowest activation energy (80.04 kJ mol^{-1}). The XPS and Soot-TPR results reveal that the catalyst $La_{0.9}K_{0.1}Co_{0.9}Cu_{0.1}O_{3-\delta}$ possesses more active and larger amount of surface oxygen species (O_2^- and O^-), more tetravalent cobalt ions and better reducibility than others, which determines its better catalytic performance. Based on *in situ* DRIFTS and other characterization results, the potential mechanisms for soot combustion, NO*x* storage and simultaneous NO*x*-soot removal are proposed.

1. Introduction

Great concerns of the diesel engines have been drawn on vehicle markets, due to their high fuel efficiency, low-operating cost and high durability. Meanwhile, attention has also grown on the negative effects of NO*x* and soot emitted by diesel engines on human health and environment [1,2]. Engine modifications can only lower the amounts of NO*x* and soot to a limited level, which cannot satisfy the more and more strict emission regulations, so advanced catalytic techniques for exhaust after-treatment should be developed to remove these two hazardous materials.

Among all kinds of technical approaches for the control of NO*x* and soot emission, simultaneous conversion of NO*x* and soot into N_2 and CO_2 in a single catalytic trap is undoubtedly the most attractive way so far [3–14]. It is first proposed by Yoshida et al. over CuO-based catalysts in oxygen-containing atmosphere [3]. Afterwards, several different types of catalysts have been developed, such as metal oxides [5,6], precious metals [7,8], spinel [9,10] and perovskite-type oxides [11–14]. Among them, perovskite-type catalysts have drawn much attention, due to their higher chemical, thermal and structural stability than the single oxides, lower cost and higher thermal stability than precious metals, and diverse catalytic performance. Perovskite structure tolerates partial substitution of both A- and B-sites cations with other elements, leading to the generation of oxygen vacancies or the change of valence of A- and/or B-site cations; as a result, the activity is often improved. When the A-site cations are partially substituted by the cations with lower valance, such as alkali metal ions, the oxidation state of B-site cations will be increased or some oxygen vacancies are generated in order to maintain the electrical neutrality. The formed higher valence ions usually possess higher catalytic activity for soot oxidation [13,14], and the formed oxygen vacancies are favorable to oxygen transferring. It is generally thought that the adsorbed oxygen species such as O_2^- and O^- often locate at oxygen vacancies on perovskites surface [15–17], which are main active oxygen species for soot combustion [17,18]. Their nature largely depends on the character of B-site ions and the substituted amount of A-site ions by lower valance ions [16]. When the A-site ions in perovskites are partially substituted by lower valance ions such as potassium ions, the catalytic activity towards NO*x*-soot reaction is often improved [19–21]. For soot oxidation in NO*x*-containing atmosphere the La-based perovskites with different B-site ions show

* Corresponding author. Tel.: +86 022 2789 2275; fax: +86 022 2789 2275.
E-mail address: mengm@tju.edu.cn (M. Meng).

0926-3373/$ – see front matter © 2012 Elsevier B.V. All rights reserved.
http://dx.doi.org/10.1016/j.apcatb.2012.03.022

the following activity order: $LaCoO_3$ > $LaMnO_3$ > $LaFeO_3$, which is almost the same as that for NO*x* reduction [22]. Oi-Uchisawa et al. ever reported that NO can be oxidized to NO_2 on Pt catalyst, and the formed NO_2 is more active for soot oxidation than NO and O_2 [23,24]. In our previous work, we found similar situation on $LaCoO_3$ catalysts [13,14], moreover, the $LaCoO_3$ perovskite exhibits higher capability for NO to NO_2 oxidation than the K/Pt/$ZrTiO_4$ catalyst [25]. Peng et al. reported that the incorporation of Cu into B-site of $LaMnO_3$ can enhance the simultaneous NO*x*-soot reaction [19,20]. However, up to now, little research focusing on K/Cu simultaneous substitution of A- and B-site cations in $LaCoO_3$ perovskite has been performed for simultaneous NO*x*-soot removal, probably due to the larger coordination radius of copper ion as compared with cobalt ion [26]. Actually, the substitution of Co by limited amount of lower valence Cu is potential, and such substitution can generate oxygen vacancies and promote the transfer of active oxygen species during the reaction. Therefore, the design of a NO*x*-soot removal catalyst based on $LaCoO_3$ perovskite with A- and B-site ions simultaneously substituted by K and Cu is feasible.

In the present work, a series of K/Cu simultaneously substituted nanostructured perovskite catalysts $La_{1-x}K_xCo_{1-y}Cu_yO_{3-\delta}$ were prepared by citric acid complexation method. The effect of K/Cu substitution on the structures and catalytic performance of the catalysts for soot combustion, NO*x* storage and simultaneous NO*x*-soot removal is carefully investigated. Based on the multiple characterizations and kinetic results, the essence of the activity enhancement arising from K/Cu substitution is discussed in detail, and the potential mechanisms for soot combustion, NO*x* storage and simultaneous soot-NO*x* removal are also proposed.

2. Experimental

2.1. Catalyst preparation

A series of nanometric perovskite catalysts $La_{1-x}K_xCo_{1-y}Cu_yO_{3-\delta}$ (x = 0, 0.1; y = 0, 0.05, 0.1, 0.2, 0.3) were prepared by citric acid complexation. $La(NO_3)_3{\cdot}6H_2O$, KNO_3, $Co(NO_3)_2{\cdot}6H_2O$ and $Cu(NO_3)_2{\cdot}3H_2O$ (Supplied by Tianjin Guangfu Fine Chemicals Research Institute) were used as precursor salts for obtaining an aqueous solution of La^{3+}, K^+, Co^{2+} and Cu^{2+} with the expected stoichiometry. A given amount of citric acid dissolved in deionized water was added in the above solution as a ligand, forming a homogeneous solution with a total concentration of 0.1 mol L^{-1} for all the cations. The molar amount of added citric acid is equal to that of all cations. The resulting solution was heated to the temperature of 80 °C under continuous stirring. The clear solution gradually turned into milky sol and finally transformed into gel, which was translucent with a honey-like color and viscosity. Then, the wet gel was dried homogenously in a stream of air at 120 °C overnight. Afterwards, the resulting loose and foamy solid was heated to 200 °C in air by an electric furnace to remove the organic ligands. Successively, the precursor was heated to 400 °C and kept for 2 h to decompose the nitrates; at last, it was calcined at 800 °C for 4 h in static air.

2.2. Catalyst characterization

X-ray diffraction measurement was recorded on an X' pert Pro rotatory diffractometer (PANAlytical Company) operating at 200 mA and 40 kV using Cu *K*α as radiation source (λ = 0.15418 nm). The data of 2θ from 10 to 90° were collected with a step size of 0.02°.

Extended X-ray absorption fine structure (EXAFS) measurements were carried out on the 1W1B beamline of Beijing Synchrotron Radiation Facility (BSRF) operating at about 150 mA and 2.2 GeV. The absorption spectra of the Co *K*-edge of the samples and reference $LaCoO_3$ were recorded at room temperature in transmission mode. A Si (1 1 1) double-crystal monochromator was used to reduce the harmonic content of the monochrome beam. The back-subtracted EXAFS function was converted into k space and weighted by k^3 in order to compensate for the diminishing amplitude due to the decay of the photoelectron wave. The Fourier transforming of the k^3-weighted EXAFS data was performed in the range of k = 3.4 to 14 $Å^{-1}$ using a Hanning function window.

The surface morphology was determined with a Hitachi S4800 field emission-scanning electron microscope (FE-SEM) instrument. An accelerating voltage of 5 kV was applied. The sample was previously coated with a very thin gold layer in order to improve the electrical conductivity of the sample surface.

Temperature-programmed reduction (TPR) was conducted on a TPDRO 1100 apparatus supplied by Thermo-Finnigan Company. Each time, 30 mg of the sample were heated from room temperature to 900 °C at a rate of 10 °C min^{-1}. A mixture gas consisting of 5 vol.% H_2 and 95 vol.% N_2 was used as reductant at a flow rate of 20 mL min^{-1}. Before detection by the TCD, the gas was purified by a trap containing CaO + NaOH materials in order to remove the H_2O and CO_2.

X-ray photoelectron spectra (XPS) were recorded with a PHI-1600 ESCA spectrometer using Mg *K*α radiation (1253.6 eV). The base pressure was 5×10^{-8} Pa. The binding energies were calibrated using C 1s peak of contaminant carbon (B.E. = 284.6 eV) as standard, and quoted with a precision of ±0.2 eV. The surface composition of the samples in terms of atomic ratios was calculated, and Gaussian–Lorentzian and Shirley background was applied for peak analysis.

A Perkin-Elmer Diamond TG/DTA instrument was used to obtain the weight loss and differential TG curves (DTG) of the samples. Each time, about 6 or 10 mg of the sample were heated at a constant rate.

In situ DRIFTS experiments were performed on a Thermo Nicolet Nexus spectrometer. The spectrometer was equipped with a MCT detector cooled by liquid nitrogen and a heating chamber allowing samples to be heated up to 600 °C. The DRIFTS spectra were recorded against a background spectrum of the sample purified just prior to introducing the adsorbates. In each run, about 15 mg of the sample in powder form were used. The NO*x* adsorption was carried out in order to reveal the NO*x* storage mechanism. Before measurement, the sample was pretreated under 10 vol.% O_2/N_2 at 300 °C for 30 min; after cooling to room temperature a background spectrum was collected, and then the sample was exposed to a flowing gas of 500 ppm NO + 10 vol.% O_2 + balance N_2. Based on 32 scans, the spectra of NO*x* adsorption from 100 to 500 °C were recorded with a spectral resolution of 4 cm^{-1}.

2.3. Activity evaluation

For soot combustion, the catalytic activity of the prepared catalysts was evaluated by TG/DTA technique using Printex-U soot purchased from Degussa as the model reactant, which possesses a specific surface area of 100 m^2 g^{-1} and an average particle size of 25 ± 3 nm (C: 92.2 wt.%; H: 0.6 wt.%; volatiles: 6 wt.%). The soot was mixed with the catalyst in a weight ratio of 1:20 in an agate mortar for 20 min to obtain a tight contact. The mixture was heated from 100 to 700 °C at a heating rate of 10 °C min^{-1} in the atmosphere of 500 ppm NO, 10 vol.% O_2 and balance N_2 with a flow rate of 100 mL min^{-1}. By comparing characteristic temperatures of TG/DTA profiles, the catalytic activity of different samples was evaluated. In this work, soot ignition temperature (denoted as T_i), soot complete conversion temperature (denoted as T_f) and that for the maximal soot combustion rate (denoted as T_m) were used to evaluate the performance of the catalysts.

For simultaneous NO*x*-soot removal, experiments were carried out in a continuous fixed-bed quartz tubular reactor (i.d. = 8 mm) mounted in a tube furnace. The reaction temperature was controlled through a PID-regulation system based on the measurements of a K-type thermocouple and varied from 100 to 700 °C at a heating rate of 10 °C min^{-1}. After the mixture of soot and catalyst (1:20, w/w) was put in the catalyst bed, and the reaction gas containing 500 ppm NO, 10 vol.% O_2 and balance N_2 with a flow rate of 120 mL min^{-1} was introduced into the reactor, giving a gas hourly space velocity (GHSV) of 36,000 h^{-1}. For comparison, in another run only 0.3 g catalyst was placed in the catalyst bed to determine the change of NO*x* concentration in the absence of soot. The concentrations of NO, NO_2 and total NO*x* from the reactor were monitored by an on-line NO–NO_2–NO*x* Analyzer (Model 42i-HL, Thermo Scientific).

2.4. Activation energy assessment

The activation energy (E_a) for soot combustion over perovskite catalysts was measured according to the Ozawa method [27,28] by using the TG/DTA technique. Each time, 6 mg of soot and catalyst mixture with mass ratio of catalyst/soot = 20:1 were analyzed during a temperature scan from 30 to 700 °C (heating rates: B = 2, 5, 10 °C min^{-1}) in the atmosphere of 500 pm NO, 10 vol.% O_2 and balance N_2 (100 mL min^{-1}). Non-catalyzed soot combustion was also carried out under the same condition in order to estimate the activation energy of non-catalyzed soot combustion.

According to the Ozawa method, the activation energy can be calculated by the following equation:

$$\ln B = -0.4567\frac{E_a}{R}\frac{1}{T} + C,$$

Here, C is a constant. If several measurements were carried out at various heating rates, the relation between $1/T$ and $\ln B$ of each pair of these data can be plotted, and the activation energy of a specimen can be obtained from the slope of the plotted line.

3. Results and discussion

3.1. Catalyst characterization

The XRD patterns of $La_{1-x}K_xCo_{1-y}Cu_yO_{3-\delta}$ perovskite catalysts are presented in Fig. 1(a). All the main diffraction peaks of the substituted samples are in good agreement with those of $LaCoO_3$ perovskite (JPCDS 48-0123), demonstrating that after substitution the ABO_3 perovskite structure is still well maintained. For the catalysts $La_{0.9}K_{0.1}CoO_{3-\delta}$ and $La_{0.9}K_{0.1}Co_{0.95}Cu_{0.05}O_{3-\delta}$, a very weak peak at 2θ = 36.9° can be detected, suggesting that a small amount of Co_3O_4 may be present, but for the K/Cu simultaneously substituted samples with higher content of Cu (y > 0.05), this diffraction peak of Co_3O_4 vanishes. The continuous increase of Cu content also makes the main diffraction peaks of the K/Cu simultaneously substituted samples decrease gradually, indicating that Cu-substitution diminishes the crystallization degree. In addition, as shown in Fig. 1(b), for all the substituted samples, the main diffraction peaks shift to lower 2θ position as compared with the unsubstituted one, especially for the K/Cu simultaneously substituted samples, whose diffraction peaks further shift to lower 2θ position with the gradual increase of Cu content. This result implies that the relatively larger K^+ and Cu^{2+} ions have been successfully incorporated into the lattice of perovskite structure [26].

Fig. 2 shows the radial structural functions (RSFs) of Co *K*-edge for the model $LaCoO_3$ and the catalysts, derived from extended X-ray absorption fine structure (EXAFS). The RSFs of the samples are very similar to that of pure $LaCoO_3$, suggesting the formation of ABO_3 perovskite in all the catalysts, which is consistent with

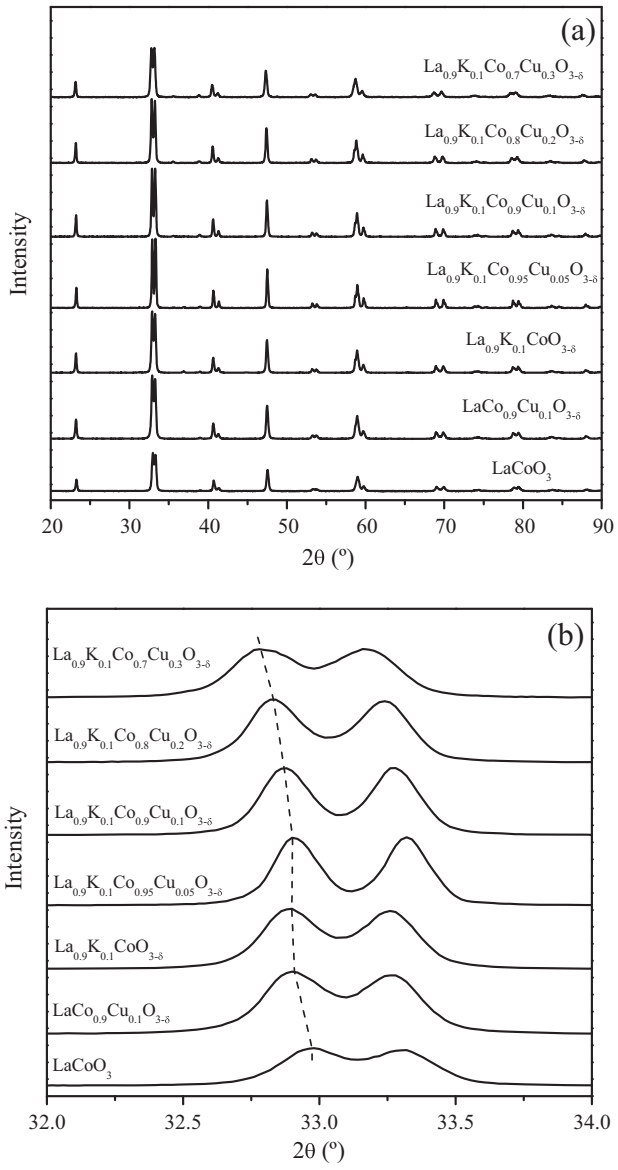

Fig. 1. XRD patterns of $La_{1-x}K_xCo_{1-y}Cu_yO_{3-\delta}$ catalysts: (a) full patterns; (b) enlarged part to show the shift of the peaks for (1 1 0) and (1 0 4) reflections.

the XRD analysis above. All the RSFs show two major coordination peaks. The first one appearing at ~1.49 Å (not corrected by phase scattering shift) is assigned to the octahedrally coordinated Co—O shell at 1.93 Å in $LaCoO_3$ perovskite structure, and the second one with the maximum around 3.17 Å is contributed by the single scattering of Co—La/Co—Co shells and multiple scattering of Co—O—Co/Co—O—Co—O shells [29]. The structural parameters for the first coordination shell (Co—O) of the catalysts from EXAFS are listed in Table 3. From Table 3, it can be seen that the coordination numbers (N) for the first Co—O shell of the K/Cu simultaneously substituted samples decrease gradually with Cu content increasing, suggesting that the crystallites of Co phases become smaller after Cu-introduction. The coordination distances (R) of Co—O shell for all the samples are almost the same as that for $LaCoO_3$ (1.93 Å) [29], which confirm that the main phases in all the samples are $LaCoO_3$ perovskite. This result is in good agreement with that of XRD.

The FT-IR spectra of $La_{1-x}K_xCo_{1-y}Cu_yO_{3-\delta}$ perovskites are displayed in Fig. 3. It is well known that the BO_6 octahedron with A-site cations in their clearance is the unit cell of ABO_3 structure.

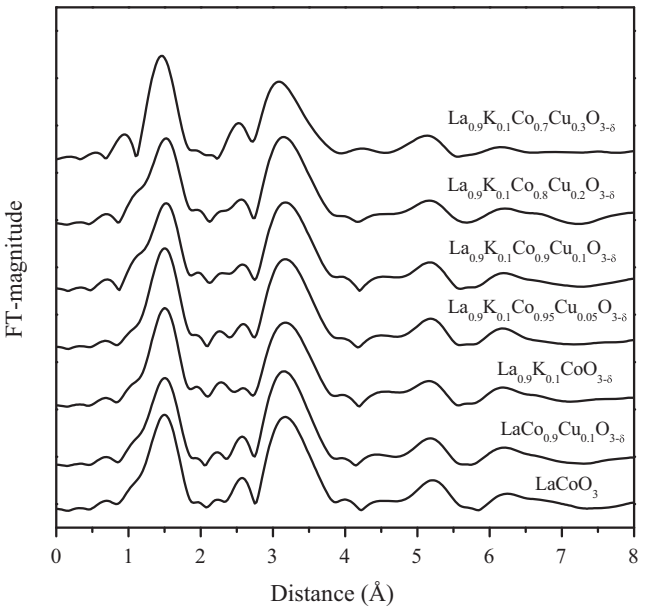

Fig. 2. Co *K*-edge radial structure functions of the catalysts derived from EXAFS.

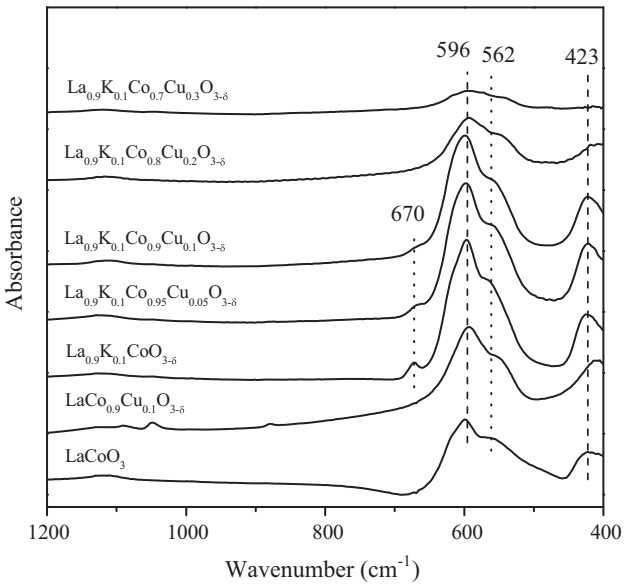

Fig. 3. FT-IR spectra of $La_{1-x}K_xCo_{1-y}Cu_yO_{3-\delta}$ catalysts.

In BO_6 unit, if three pairs of B—O bonds have the same length, namely, the BO_6 octahedron possessing high symmetry, the symmetric stretching vibration (ν_3) is IR inactive. On the contrary, the B—O stretching vibration is IR active when the symmetry of BO_6 is decreased [30]. In Fig. 3, there are three vibration bands appearing at 596, 562, 423 cm^{-1} for all the samples. The bands at 596 and 562 cm^{-1} are assigned to two kinds of stretching vibration of Co—O bond in the CoO_6 octahedron, and the band at 423 cm^{-1} is attributed to Co—O bending vibration in the CoO_6 octahedron [31]. These results further prove that the prepared catalysts have formed well ABO_3 perovskite structure. A very weak band at 670 cm^{-1}, which corresponds to Co_3O_4 phase [32], is also detected for the K-containing catalysts $La_{0.9}K_{0.1}CoO_{3-\delta}$, $La_{0.9}K_{0.1}Co_{0.95}Cu_{0.05}O_{3-\delta}$ and $La_{0.9}K_{0.1}Co_{0.9}Cu_{0.1}O_{3-\delta}$; with the introduction of Cu to the perovskite, this band decreases; when the amount of Cu exceeds 10% ($y > 0.1$), it totally disappears. This result is in good consistence with those of XRD and EXAFS.

The morphology of $La_{1-x}K_xCo_{1-y}Cu_yO_{3-\delta}$ perovskites is displayed in Fig. 4. It can be seen that for the unsubstituted $LaCoO_3$

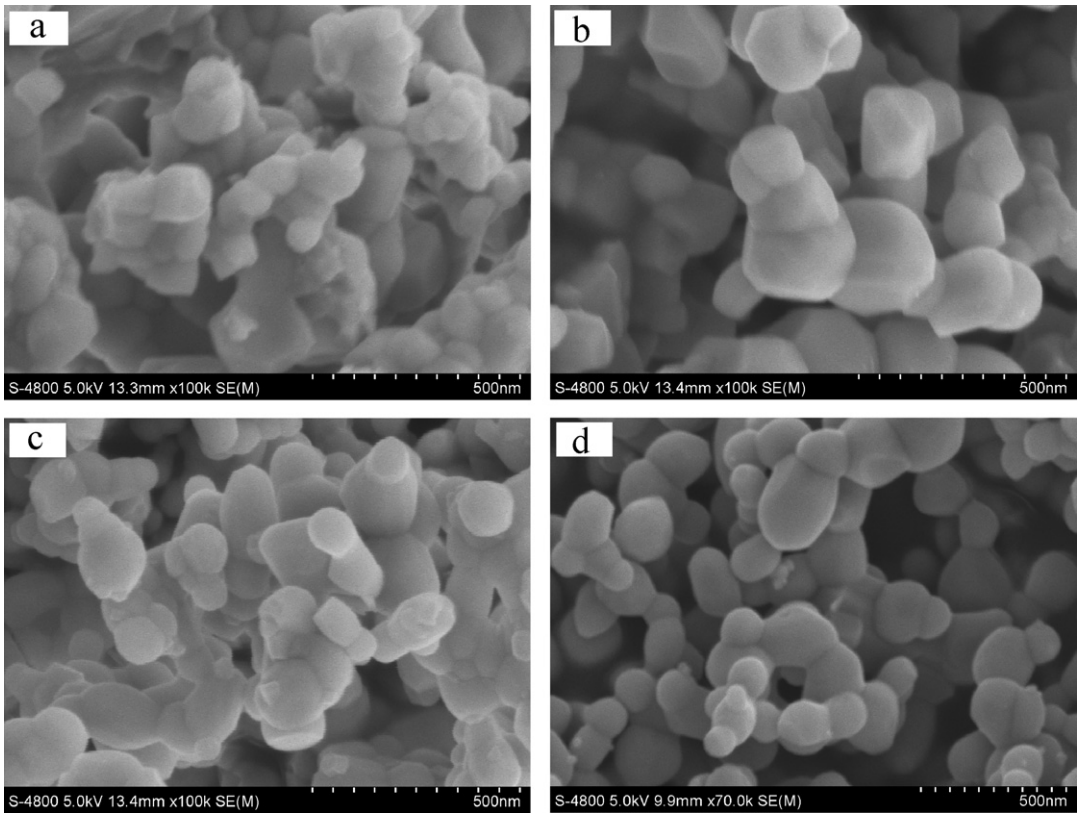

Fig. 4. FE-SEM photographs of $La_{1-x}K_xCo_{1-y}Cu_yO_{3-\delta}$ catalysts: (a) $LaCoO_3$; (b) $La_{0.9}K_{0.1}CoO_{3-\delta}$; (c) $LaCo_{0.9}Cu_{0.1}O_{3-\delta}$; (d) $La_{0.9}K_{0.1}Co_{0.9}Cu_{0.1}O_{3-\delta}$.

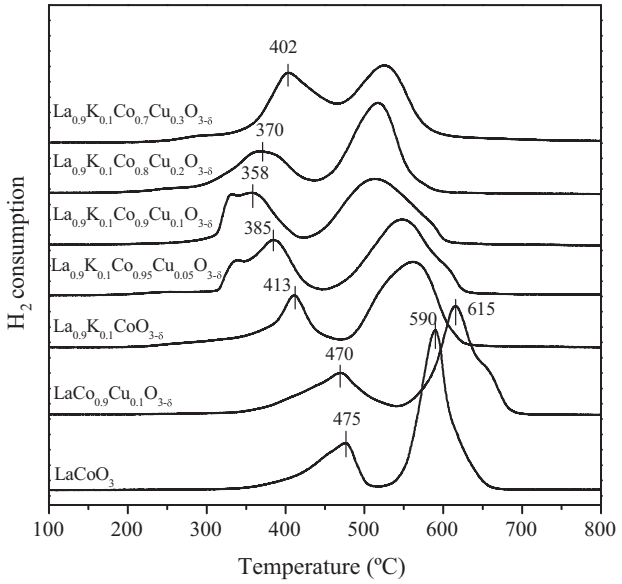

Fig. 5. H_2-TPR profiles of $La_{1-x}K_xCo_{1-y}Cu_yO_{3-\delta}$ catalysts.

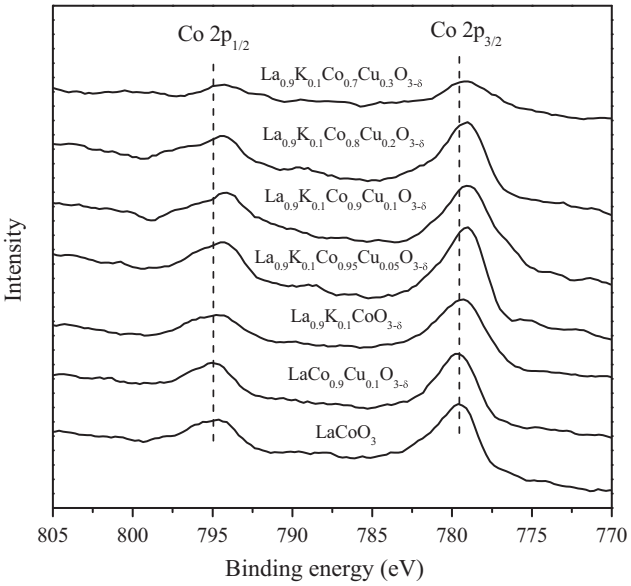

Fig. 6. XPS spectra of Co 2p core level for $La_{1-x}K_xCo_{1-y}Cu_yO_{3-\delta}$ catalysts.

and K-substituted $La_{0.9}K_{0.1}CoO_{3-\delta}$, the shapes of perovskite particles are not uniform with the particles gathering together to some extent, as presented in Fig. 4(a) and (b). However, after introduction of Cu into the catalysts, as seen in Fig. 4(c) and (d), the situation is different, especially for the K/Cu simultaneously substituted sample, which shows smaller and more uniform sphere-like particles. The average size of the $La_{0.9}K_{0.1}Co_{0.9}Cu_{0.1}O_{3-\delta}$ perovskite crystallites is about 100–120 nm, close to that for diesel soot particulates (70–100 nm) [33], which is favorable to achieving the highest specific number of contact points between the two counterparts. Due to the big size of soot particulates, the inner surface in the pores of perovskite catalysts is not accessible to them. As a result, the outer surface of the catalysts is rather important during soot combustion and NO*x*-soot reaction, which provides the necessary solid–solid contact sites [34].

The reducibility of the catalysts was characterized by H_2-TPR, as presented in Fig. 5. It can be seen that for $LaCoO_3$ there are two main reduction peaks, appearing at about 475 and 590 °C, respectively. Both Wachowski et al. [35] and Engelmann-Pirez et al. [36] thought that the first one corresponds to a partial reduction of $LaCoO_3$ to an oxygen-deficient perovskite (La_2CoO_4), and the second one is the complete reduction of La_2CoO_4 to Co^0 and La_2O_3. When only Cu is introduced into $LaCoO_3$ perovskite, no big change for the first reduction peak (470 °C) is observed, on the contrary, the reduction for second one is obviously delayed. However, as K is introduced into $LaCoO_3$ the reduction temperature of the first peak is decreased more than 60 °C; and that for the second one is also decreased to some extent. After simultaneously substituted by K and Cu, the reduction temperature is further lowered, which exhibits a volcano-type tendency with the increase of Cu content. Apparently, the optimal substituted amount of Cu is $y = 0.1$. In a summary, the reducibility for these perovskite catalysts changes in the following sequence: $La_{0.9}K_{0.1}Co_{0.9}Cu_{0.1}O_{3-\delta} > La_{0.9}K_{0.1}Co_{0.8}Cu_{0.2}O_{3-\delta} > La_{0.9}K_{0.1}Co_{0.95}Cu_{0.05}O_{3-\delta} > La_{0.9}K_{0.1}Co_{0.7}Cu_{0.3}O_{3-\delta} > La_{0.9}K_{0.1}CoO_{3-\delta} > LaCo_{0.9}Cu_{0.1}O_{3-\delta} \approx LaCoO_3$.

Fig. 6 and Table 1 display the XPS results of Co 2p for the $La_{1-x}K_xCo_{1-y}Cu_yO_{3-\delta}$ catalysts. All the Co 2p spectra exhibit two main peaks corresponding to the Co $2p_{1/2}$ and Co $2p_{3/2}$ levels. The binding energy of Co $2p_{3/2}$ of the unsubstituted $LaCoO_3$ catalyst and the Cu-substituted one ($LaCo_{0.9}Cu_{0.1}O_{3-\delta}$) is 779.6 eV, which is close to the value reported in the literature [37,38] and also equivalent roughly to the binding energy of Co $2p_{3/2}$ in Co_2O_3 (779.6 eV) [39]; this suggests that most of cobalt ions in $LaCoO_3$ and $LaCo_{0.9}Cu_{0.1}O_{3-\delta}$ should be present as trivalent cations. In the K-substituted catalyst ($La_{0.9}K_{0.1}CoO_{3-\delta}$), the Co $2p_{3/2}$ peak shifts to lower binding energy (779.3 eV) due to the electron-donor effect of basic component K. Since the valence of K is lower than that of La, the substitution of La by K will lead to the formation of higher oxidation state of B-site ions (such as Co^{3+} to Co^{4+}), and/or the formation of oxygen vacancies so that the electrical neutrality of the perovskite can be maintained. It is reported that the formation of Co^{4+} can induce the shift of binding energy toward lower value [37]. So, the decrease of Co $2p_{3/2}$ binding energy for $La_{0.9}K_{0.1}CoO_{3-\delta}$ catalyst means that some Co^{3+} ions have transformed into Co^{4+}; however, the presence of oxygen vacancies cannot be excluded, which will be elucidated in the next part for the XPS results of O 1s. After simultaneously substituted by K and Cu, the binding energy of Co $2p_{3/2}$ for the catalysts is further lowered to 779.0 eV, suggesting that more Co^{4+} ions and/or more oxygen vacancies have formed.

The XPS spectra of O 1s for the $La_{1-x}K_xCo_{1-y}Cu_yO_{3-\delta}$ catalysts are shown in Fig. 7. It is found that there are two binding energy peaks in each spectrum, corresponding to two kinds of oxygen species. The O 1s peak with low binding energy (~528.5 eV) is attributed to surface lattice oxygen, and the other one with higher binding energy (~531.3 eV) is assigned to surface adsorbed oxygen species such as O_2^- or O^-. Generally, the surface oxygen species are generated through the adsorption of gaseous O_2 on the oxygen vacancies existing in defected

Table 1
Binding energies (BE) of Co $2p_{3/2}$ and O 1s core levels and the percentages of different kinds of surface oxygen species for the catalysts $La_{1-x}K_xCo_{1-y}Cu_yO_{3-\delta}$.

Catalysts	BE of Co $2p_{3/2}$ (eV)	BE of O 1s (eV)	Percentages (%)
$LaCoO_3$	779.6	528.5[a]/531.3[b]	47[a]/53[b]
$LaCo_{0.9}Cu_{0.1}O_{3-\delta}$	779.6	529.4[a]/531.9[b]	46[a]/54[b]
$La_{0.9}K_{0.1}CoO_{3-\delta}$	779.3	528.3[a]/531.0[b]	42[a]/58[b]
$La_{0.9}K_{0.1}Co_{0.95}Cu_{0.05}O_{3-\delta}$	779.0	528.7[a]/531.3[b]	38[a]/62[b]
$La_{0.9}K_{0.1}Co_{0.9}Cu_{0.1}O_{3-\delta}$	779.0	528.5[a]/531.3[b]	36[a]/64[b]
$La_{0.9}K_{0.1}Co_{0.8}Cu_{0.2}O_{3-\delta}$	779.0	528.6[a]/531.4[b]	37[a]/63[b]
$La_{0.9}K_{0.1}Co_{0.7}Cu_{0.3}O_{3-\delta}$	779.0	528.7[a]/531.2[b]	40[a]/60[b]

[a] Surface lattice oxygen.
[b] Surface adsorbed oxygen.

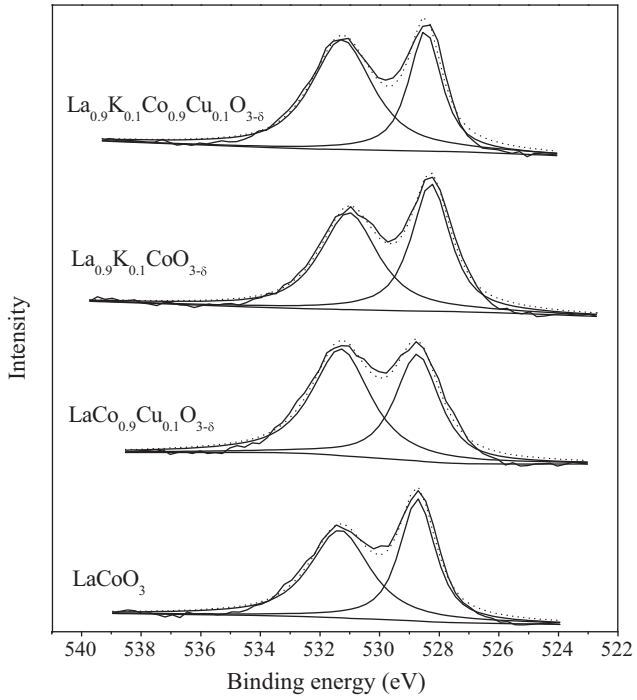

Fig. 7. XPS spectra of O 1s core level for $La_{1-x}K_xCo_{1-y}Cu_yO_{3-\delta}$ catalysts.

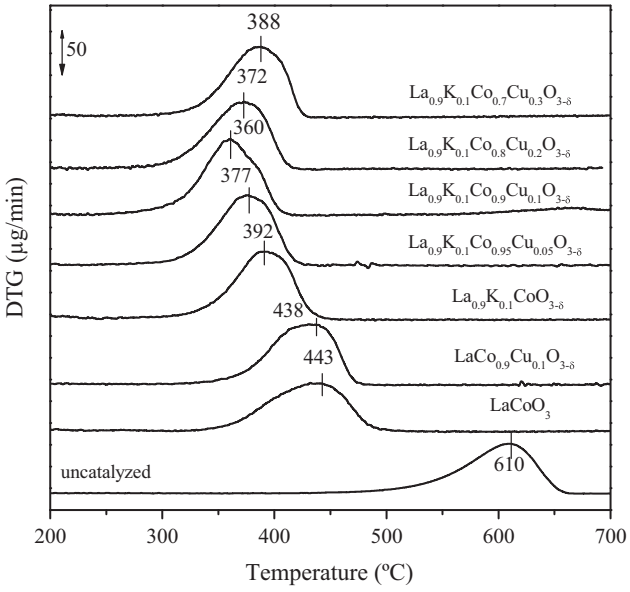

Fig. 8. DTG profiles of soot combustion in the atmosphere of 500 ppm NO + 10 vol.% O_2 + balanced N_2 over $La_{1-x}K_xCo_{1-y}Cu_yO_{3-\delta}$ catalysts.

oxides [40–42]. The presence of surface adsorbed oxygen species suggests the formation of oxygen vacancies on the perovskite catalysts. Since the O 1s peaks in Fig. 7 are not symmetric, they are fitted by a standard Gaussian–Lorentzian deconvolution to get a relative content of different oxygen species. The deconvolution results are listed in Table 1. It can be seen that after simultaneous substitution by K and Cu, the catalysts possess higher percentage of surface adsorbed oxygen species, which indirectly indicates the formation of more oxygen vacancies on the simultaneously substituted catalysts. According to the data in Table 1, the relative amounts of surface adsorbed oxygen species for different catalysts can be arranged in the following order: $La_{0.9}K_{0.1}Co_{0.9}Cu_{0.1}O_{3-\delta} > La_{0.9}K_{0.1}Co_{0.8}Cu_{0.2}O_{3-\delta} \approx La_{0.9}K_{0.1}Co_{0.95}Cu_{0.05}O_{3-\delta} > La_{0.9}K_{0.1}Co_{0.7}Cu_{0.3}O_{3-\delta} > La_{0.9}K_{0.1}CoO_{3-\delta} > LaCo_{0.9}Cu_{0.1}O_{3-\delta} \approx LaCoO_3$. Obviously, the catalyst $La_{0.9}K_{0.1}Co_{0.9}Cu_{0.1}O_{3-\delta}$ possesses the largest amount of surface adsorbed oxygen species as well as the largest amount of oxygen vacancies.

3.2. Catalytic soot combustion over $La_{1-x}K_xCo_{1-y}Cu_yO_{3-\delta}$ catalysts

The performance of $La_{1-x}K_xCo_{1-y}Cu_yO_{3-\delta}$ catalysts for soot combustion in the atmosphere of 500 ppm NO, 10 vol.% O_2 and balance N_2 is shown in Fig. 8 and Table 2. For comparison, the result of uncatalyzed soot combustion is also presented in Fig. 8. It is obvious that without catalysts the soot oxidation starts from 438 °C with the zenith appearing at the high temperature of 610 °C, which corresponds to the maximal soot combustion rate (T_m). When the $LaCoO_3$ catalyst is loaded, the T_m is lowered by about 170 °C. After introduction of 10% ($y = 0.1$) copper into $LaCoO_3$, the T_m is only decreased by 6 °C. However, the introduction of K can lower the T_m at least 51 °C as compared with that for $LaCoO_3$. The simultaneous introduction of K and Cu into $LaCoO_3$ can further decrease the T_m, and with the increase of Cu amount this temperature exhibits volcano-type tendency. The lowest T_m (360 °C) is observed on $La_{0.9}K_{0.1}Co_{0.9}Cu_{0.1}O_{3-\delta}$ catalyst. According to the T_m, the catalytic activity of $La_{1-x}K_xCo_{1-y}Cu_yO_{3-\delta}$ catalysts for soot combustion can be arranged in the following sequence:

Table 2
Characteristic temperature for the maximal soot combustion rate (T_m), the activation energy for soot combustion (E_a), the NO*x* storage capacity (NSC) and NO*x* reduction percentage (NRP) of $La_{1-x}K_xCo_{1-y}Cu_yO_{3-\delta}$ catalysts.

Catalysts	T_m (°C)	E_a (kJ mol^{-1})	NSC (μmol g^{-1})	NRP (%)
$LaCoO_3$	443	107.7	102	11
$LaCo_{0.9}Cu_{0.1}O_{3-\delta}$	438	107.0	113	13
$La_{0.9}K_{0.1}CoO_{3-\delta}$	392	100.7	140	13
$La_{0.9}K_{0.1}Co_{0.95}Cu_{0.05}O_{3-\delta}$	377	85.19	190	17
$La_{0.9}K_{0.1}Co_{0.9}Cu_{0.1}O_{3-\delta}$	360	84.02	284	32
$La_{0.9}K_{0.1}Co_{0.8}Cu_{0.2}O_{3-\delta}$	372	85.16	270	26
$La_{0.9}K_{0.1}Co_{0.7}Cu_{0.3}O_{3-\delta}$	388	91.76	256	23
Uncatalyzed	610	139.7	–	–

$La_{0.9}K_{0.1}Co_{0.9}Cu_{0.1}O_{3-\delta} > La_{0.9}K_{0.1}Co_{0.8}Cu_{0.2}O_{3-\delta} \approx La_{0.9}K_{0.1}Co_{0.95}Cu_{0.05}O_{3-\delta} > La_{0.9}K_{0.1}Co_{0.7}Cu_{0.3}O_{3-\delta} \approx La_{0.9}K_{0.1}CoO_{3-\delta} > LaCo_{0.9}Cu_{0.1}O_{3-\delta} \approx LaCoO_3$.

The above XRD, EXAFS and FT-IR results have indicated that the major phases in the as-prepared catalysts are perovskite-type oxides, though a very small amount of Co_3O_4 is also identified in K-containing samples. Therefore, it is believed that the perovskite oxides are the main active phases for soot combustion, as reported in literature [32]. In soot combustion system, there are two solid phases, namely catalyst and soot, and a gaseous phase (O_2 and NO*x*); the soot oxidation should occur at the triple-phase

Table 3
Structure parameters of the first Co—O coordination shell of the $La_{1-x}K_xCo_{1-y}Cu_yO_{3-\delta}$ catalysts from EXAFS.

Catalysts	Shell	R (Å)[a]	N[b]	$\Delta\sigma^2 \times 10^{-5}$ (Å^2)[c]	Residual (%)
$LaCoO_3$	Co—O	1.93	5.3	3.6	3.6
$LaCo_{0.9}Cu_{0.1}O_{3-\delta}$	Co—O	1.93	5.6	2.3	4.2
$La_{0.9}K_{0.1}CoO_{3-\delta}$	Co—O	1.92	5.6	4.2	5.0
$La_{0.9}K_{0.1}Co_{0.95}Cu_{0.05}O_{3-\delta}$	Co—O	1.93	5.7	3.7	6.8
$La_{0.9}K_{0.1}Co_{0.9}Cu_{0.1}O_{3-\delta}$	Co—O	1.91	5.6	5.6	7.3
$La_{0.9}K_{0.1}Co_{0.8}Cu_{0.2}O_{3-\delta}$	Co—O	1.92	5.5	7.3	7.9
$La_{0.9}K_{0.1}Co_{0.7}Cu_{0.3}O_{3-\delta}$	Co—O	1.92	5.4	6.4	8.6

[a] Coordination distance.
[b] Coordination number.
[c] Debye–Waller factor.

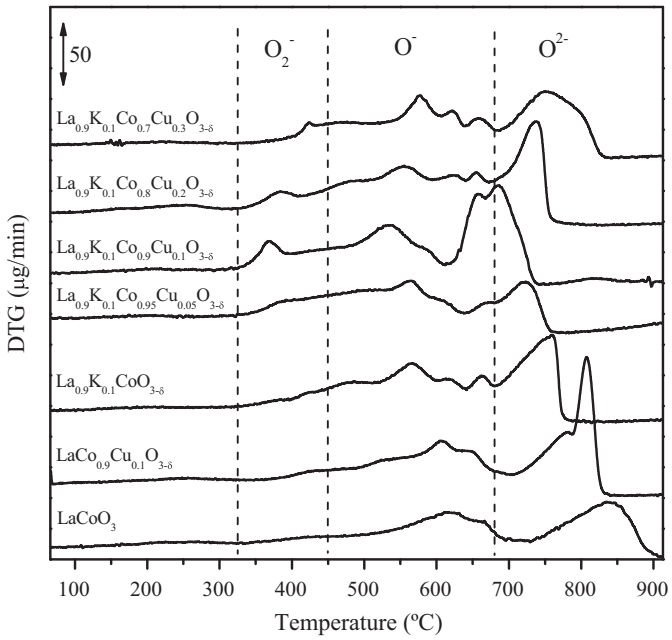

Fig. 9. DTG profiles of soot oxidation in highly pure N_2 (99.99%) over the catalysts $La_{1-x}K_xCo_{1-y}Cu_yO_{3-\delta}$.

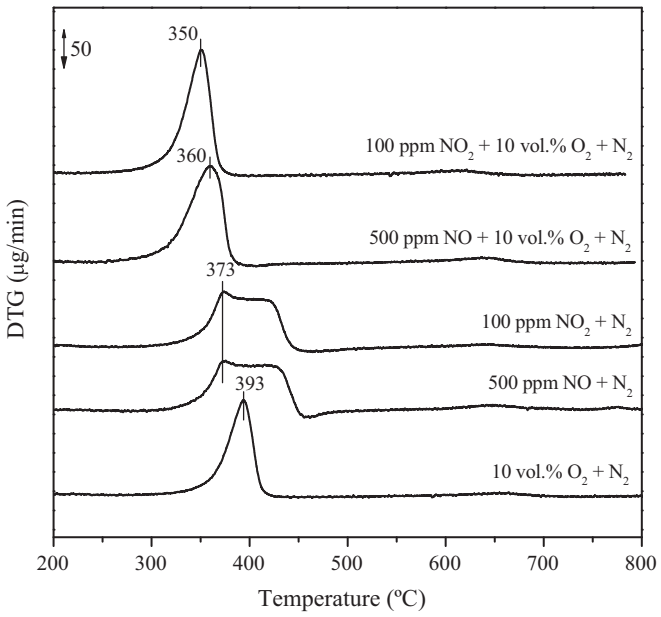

Fig. 10. DTG profiles of soot combustion in different atmospheres over the catalyst $La_{0.9}K_{0.1}Co_{0.9}Cu_{0.1}O_{3-\delta}$.

boundary. So, the contact conditions between soot and the catalytic active sites are extremely important for this kind of reactions [43–45]. Liu et al. [34] even thought that the contact conditions between catalysts and soot is a rate-determining factor because the number of contact points on the catalysts is proportional to the concentration of active sites. Based upon this analysis and above characterization results, in this work, the high activity for soot combustion of the K/Cu simultaneously substituted perovskite catalysts can be assigned to the following aspects. Firstly, the crystallites of nanometric $La_{1-x}K_xCo_{1-y}Cu_yO_{3-\delta}$ catalysts possess more uniform particle size (100–120 nm), close to that of soot, which is favorable to achieving high contacting efficiency between the two counterparts. Secondly, the cobalt ions in K/Cu simultaneously substituted catalysts $La_{0.9}K_{0.1}Co_{1-y}Cu_yO_{3-\delta}$ show higher reducibility as compared with those in $LaCoO_3$ and single substituted samples, which facilitates the redox circulation during soot combustion, thus increasing the catalytic activity. Thirdly, as revealed by Co 2p XPS results, the presence of more Co^{4+} ions in the K/Cu simultaneously substituted catalysts makes them possess higher oxidation ability, lowering the soot oxidation temperature. Fourthly, simultaneous substitution of La/Co by K/Cu enhances the formation of more oxygen vacancies in $La_{0.9}K_{0.1}Co_{1-y}Cu_yO_{3-\delta}$, as reflected by the larger amount of adsorbed oxygen species detected by XPS; the presence of more oxygen vacancies accelerates the transferring of oxygen species during soot combustion [17,34].

To further investigate the reactivity of different oxygen species during soot combustion, the temperature-programmed soot oxidation was performed in highly pure N_2 (99.99%) atmosphere. In this process, the soot can only be oxidized by the oxygen species existing on the catalyst surface such as surface adsorbed and lattice oxygen species, accompanied by the reduction of metallic ions in the catalysts, so, this process is also called Soot-TPR technique. Fig. 9 displays the Soot-TPR profiles of different catalysts. It can be seen that there are mainly three kinds of oxygen species, which are attributed to O_2^- (320–450 °C), O^- (450–680 °C) and O^{2-} (>680 °C) [17,34], respectively. According to the temperature range of soot combustion in Fig. 8, O_2^- and O^- species are the main active oxygen species for soot combustion. From Fig. 9, it can still be found that the K/Cu simultaneously substituted catalysts, especially the $La_{0.9}K_{0.1}Co_{0.9}Cu_{0.1}O_{3-\delta}$, possess much larger amount of O_2^- species than others; in addition, the O_2^- and O^- species in K/Cu simultaneously substituted catalysts show lower reduction temperatures and higher reactivity with soot as compared with those in other catalysts.

To clarify the role of NO in the reaction, soot combustion was carried out over $La_{0.9}K_{0.1}Co_{0.9}Cu_{0.1}O_{3-\delta}$ catalyst under several different atmospheres (500 ppm NO + N_2, 100 ppm NO_2 + N_2, 10 vol.% O_2 + N_2, 500 ppm NO + 10 vol.% O_2 + N_2, 100 ppm NO_2 + 10 vol.% O_2 + N_2), as shown in Fig. 10. In the absence of NO*x* (N_2 + 10 vol.% O_2), the characteristic temperature T_m is 393 °C. When NO or NO_2 is present (500 ppm NO + N_2, 100 ppm NO_2 + N_2), the soot combustion is enhanced, showing a lower T_m of 373 °C. It suggests that NO*x* species are more active for soot oxidation than oxygen. According to literature [23,46], NO can be oxidized to NO_2 by surface oxygen species (O_2^-, O^-) and gaseous O_2, which shows higher reactivity for soot oxidation than NO and O_2. So, it is deduced that during soot combustion some NO may be first oxidized to NO_2, then reacts with soot; as a result, they show similar profiles for soot oxidation as shown in Fig. 10. In the coexistence of NO*x* and oxygen (500 ppm NO + 10 vol.% O_2 + N_2, 100 ppm NO_2 + 10 vol.% O_2 + N_2), the soot combustion rate is further increased, giving more and more lower characteristic temperatures of T_m (360 and 350 °C, respectively). In a summary, the presence of NO*x* is favorable to soot combustion; the oxidation of soot by NO is probably *via* NO_2 intermediate [23,24,46].

In order to better understand the performance of different catalysts for soot combustion, kinetic experiments were carried out and the activation energy was calculated, as listed in Table 2. It is obvious that the activation energy for catalyzed soot combustion is much lower than that without using catalysts. For pure $LaCoO_3$ and K or Cu single substituted samples, the activation energy is close to each other. After simultaneous substitution of La/Co by K/Cu, the activation energy of soot combustion is lowered to a significant extent. For the most active catalyst $La_{0.9}K_{0.1}Co_{0.9}Cu_{0.1}O_{3-\delta}$, the activation energy is only 84.02 kJ mol^{-1}. Combined with the above characterization results, it is believed that the obvious decrease of activation energy should be highly related to the generation of more oxygen vacancies, the presence of more active and larger amount of surface adsorbed oxygen species, the formation of more Co^{4+}

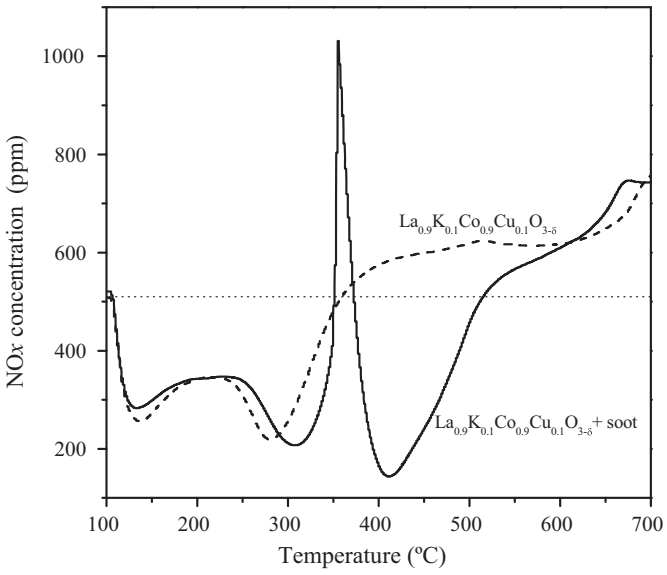

Fig. 11. Profiles of NO*x* storage in the atmosphere of 500 ppm NO + 10 vol.% O_2 + balance N_2 over $La_{0.9}K_{0.1}Co_{0.9}Cu_{0.1}O_{3-\delta}$ catalyst in the absence or presence of soot.

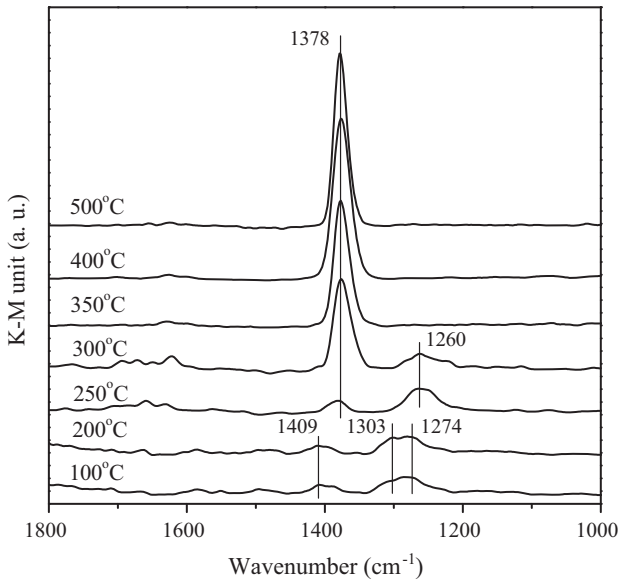

Fig. 12. *In situ* DRIFT spectra of NO*x* sorption on $La_{0.9}K_{0.1}Co_{0.9}Cu_{0.1}O_{3-\delta}$ catalyst in the atmosphere of 500 pm NO + 10 vol.% O_2 + balance N_2.

ions and the better reducibility of this catalyst. The much better catalytic performance for soot combustion of the K/Cu simultaneously substituted catalysts can be well correlated with their much lower activation energy.

3.3. NOx storage and reduction over $La_{1-x}K_xCo_{1-y}Cu_yO_{3-\delta}$ catalysts

The profile for NO*x* storage on the catalyst $La_{0.9}K_{0.1}Co_{0.9}Cu_{0.1}O_{3-\delta}$ is presented in Fig. 11 (dash line). The value of the starting point in each curve represents the NO*x* concentration in the feed; the points below or above this value mean the occurrence of NO*x* sorption and desorption, respectively. From Fig. 11, two major storage periods are observed; one is from room temperature to about 220 °C, and the other is between 220 and 350 °C, which correspond to the surface storage and bulk storage, respectively. It should be noted that at higher temperature (>350 °C), the NO*x* concentration is becoming larger and larger as compared with that in the feed, which is resulted from the decomposition of storage species, such as nitrate and/or nitrite species. The amounts of NO*x* uptake for all the catalysts are calculated from the peak area of the absorption curves, which are listed in Table 2. It can be seen that the K/Cu simultaneously substituted samples possess larger NO*x* storage capacity (NSC) than the others. In literature [47–50], it has been confirmed that the formation of NO_2 is the first and crucial step for NO*x* storage, so, the oxidation ability of the catalysts should be highly related to their NO*x* storage performance. As revealed by XPS and Soot-TPR above, the K/Cu simultaneously substituted catalysts possess more Co^{4+} ions, more active and higher content of surface adsorbed O_2^- and O^- species, all of which are favorable to the oxidation of NO to NO_2, thus enhancing the NSC of these catalysts. The NSC for different catalysts shows the following order: $La_{0.9}K_{0.1}Co_{0.9}Cu_{0.1}O_{3-\delta} > La_{0.9}K_{0.1}Co_{0.8}Cu_{0.2}O_{3-\delta} > La_{0.9}K_{0.1}Co_{0.7}Cu_{0.3}O_{3-\delta} > La_{0.9}K_{0.1}Co_{0.95}Cu_{0.05}O_{3-\delta} > La_{0.9}K_{0.1}CoO_{3-\delta} > LaCo_{0.9}Cu_{0.1}O_{3-\delta} \approx LaCoO_3$.

For better understanding the NO*x* storage behavior of the catalysts, *in situ* DRIFTS experiments were carried out to figure out the NO*x* storage pathway, as shown in Fig. 12. It can be found that in the first storage stage (100–200 °C), NO*x* is mainly stored as monodentate/bridged bidentate nitrate species (1409 and 1303 cm^{-1}), and chelating bidentate nitrate species (1274 cm^{-1}) [4,51]. In the second stage (250–300 °C), NO*x* is mainly stored as ionic nitrate species (1378 cm^{-1}) and bidentate nitrite species (1260 cm^{-1}) [51,52]. With the temperature increasing to 350 °C or above, only free ionic nitrate species (1378 cm^{-1}) are observed.

In order to investigate the behavior of the catalysts for simultaneous NO*x*-soot removal, the mixture of catalyst and soot was loaded to the catalyst-bed for a same temperature-programmed heating in the same stream as that for NO*x* storage on pure catalyst. Taking the mixture of soot/$La_{0.9}K_{0.1}Co_{0.9}Cu_{0.1}O_{3-\delta}$ as an example, its NO*x* concentration profile during the heating process is recorded and also displayed in Fig. 11 (solid line) for a comparison with that of $La_{0.9}K_{0.1}Co_{0.9}Cu_{0.1}O_{3-\delta}$ alone. From Fig. 11, it can be seen that the soot/$La_{0.9}K_{0.1}Co_{0.9}Cu_{0.1}O_{3-\delta}$ mixture and $La_{0.9}K_{0.1}Co_{0.9}Cu_{0.1}O_{3-\delta}$ show very similar NO*x* uptake performance at low temperature region (<350 °C), but a noticeable difference exists at higher temperature region. Unlike the case for $La_{0.9}K_{0.1}Co_{0.9}Cu_{0.1}O_{3-\delta}$ alone, a very sharp NO*x* desorption peak appears at 356 °C, just after the onset of soot combustion, referring to the DTG profile of soot combustion in Fig. 8. So, it is thought that the large amount of the released NO*x* comes from the decomposition of nitrate and/or nitrite species, which is facilitated by the strong exotherm of soot combustion. After this, NO*x* concentration suddenly decreases to the level under the dotted baseline, evidencing the occurrence of NO*x* reduction by soot. Moreover, judging from the observed areas below and above the dotted baseline, the amounts of NO*x* sorption and desorption for $La_{0.9}K_{0.1}Co_{0.9}Cu_{0.1}O_{3-\delta}$ were almost the same. However, for soot/$La_{0.9}K_{0.1}Co_{0.9}Cu_{0.1}O_{3-\delta}$ mixture, the observed area below the dotted line is much larger than that above it, corresponding to 311 and 76 μmol of NO*x* per gram catalyst, respectively. This significant difference suggests that partial NO*x* has been reduced by soot during the heating process. Based upon this analysis, the NO*x* reduction percentages over different catalysts are calculated and listed in Table 2. It can be seen that the NO*x* reduction percentages over the K/Cu simultaneously substituted catalysts are much larger than those over $LaCoO_3$ and single substituted catalysts; the $La_{0.9}K_{0.1}Co_{0.9}Cu_{0.1}O_{3-\delta}$ catalyst possesses the highest NO*x* reduction percentage of 32%. It is reported [4,52] that the NO*x* reduction by soot generally consists of several steps: (1) NO is adsorbed and oxidized to NO_2 by the catalyst, (2) NO or NO_2 is stored as nitrites and/or nitrates, (3) with the increase of

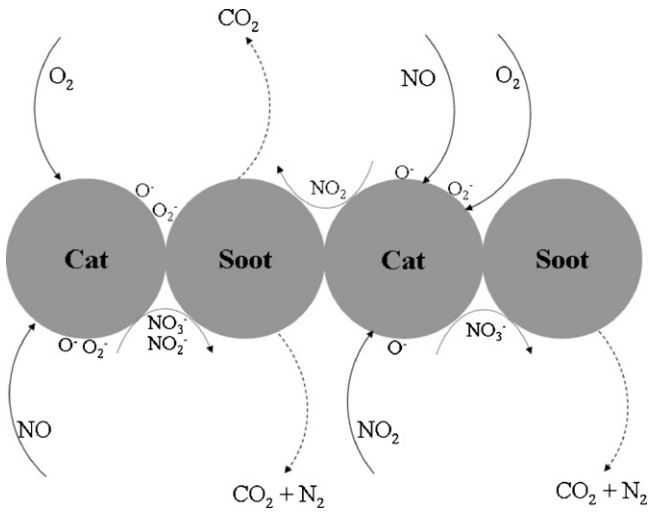

Fig. 13. Scheme of the reaction mechanisms for the simultaneous NO*x*-soot removal over $La_{1-x}K_xCo_{1-y}Cu_yO_{3-\delta}$ catalysts.

temperature, the soot is ignited, giving out a lot of heat, which facilitates the decomposition of formed nitrites or nitrates, at the same time, the released NO*x* can be partially reduced by soot. The largest contents of Co^{4+} ions and surface adsorbed oxygen species, and the best reducibility of the catalyst $La_{0.9}K_{0.1}Co_{0.9}Cu_{0.1}O_{3-\delta}$ determine its best catalytic performance for simultaneous removal of soot and NO*x*.

Combined with all the results and analysis, a potential mechanism scheme for simultaneous soot-NO*x* removal is proposed, as shown in Fig. 13. There are mainly four reaction pathways: (1) soot oxidation on the solid–solid interface of the catalyst and soot by the active O_2^- and O^- species which can be continuously supplemented by gaseous O_2 through the oxygen vacancies; (2) NO oxidation to NO_2 on catalyst surface forming surface adsorbed species, which migrate to solid–solid boundary and oxidize the soot; (3) adsorption and oxidation of gaseous NO to nitrite and/or nitrate species, which can oxidize the soot and give out the products CO_2 and N_2; (4) adsorption and oxidation of gaseous NO_2 to nitrate species, which can directly react with soot or decompose into NO*x* species during heating to take part in soot oxidation. Herein, it should be noted that for all the catalytic systems only N_2 is detected during NO*x* reduction by soot, no N_2O species are found. In addition, for soot oxidation only traces of CO are detected in the effluent gas, the selectivity of CO_2 for all catalysts is always higher than 99.5%; the catalyst $La_{0.9}K_{0.1}Co_{0.9}Cu_{0.1}O_{3-\delta}$ exhibits the largest CO_2 selectivity of 99.8%, showing the strongest total oxidation ability. In a summary, the K/Cu simultaneously substituted perovskite catalysts $La_{1-x}K_xCo_{1-y}Cu_yO_{3-\delta}$, especially $La_{0.9}K_{0.1}Co_{0.9}Cu_{0.1}O_{3-\delta}$, are highly efficient multifunctional catalysts used for soot combustion, NO*x* storage and simultaneous NO*x*-soot removal.

4. Conclusions

The K/Cu simultaneously substituted perovskite catalysts $La_{1-x}K_xCo_{1-y}Cu_yO_{3-\delta}$ possess much higher catalytic performance towards soot combustion, NO*x* storage and simultaneous NO*x*-soot removal as compared with unsubstituted $LaCoO_3$ and K or Cu single substituted perovskite catalysts. Among all the catalysts, the nanometric $La_{0.9}K_{0.1}Co_{0.9}Cu_{0.1}O_{3-\delta}$ with the crystallite size of 100–120 nm, exhibits the highest catalytic activity, showing the lowest soot combustion characteristic temperature (T_m) of 360 °C, the highest NO*x* storage capacity (NSC) of 284 μmol g^{-1} and the highest NO*x* reduction percentage of 32%.

The K/Cu simultaneous substitution facilitates the formation of more oxygen vacancies, larger amount of surface adsorbed oxygen species and more Co^{4+} ions, which makes the perovskites possess much better redox properties. The surface O_2^- and O^- species are the main active oxygen species for soot combustion and NO oxidation to NO_2 during NO*x* storage. Several kinds of NO*x* adsorption and storage species are identified such as bidentate nitrite, monodentate nitrate, bridged bidentate nitrate, chelating bidentate nitrate, and ionic nitrate species, but above 300 °C, only ionic nitrate species are detected. The simultaneous NO*x*-soot removal mainly takes place at the temperature higher than 350 °C through the intermediates of nitrate and its decomposition product NO_2. The kinetic experiment and calculation results show that the activation energy for soot combustion is remarkably lowered by the simultaneous substitution of La^{3+}/Co^{3+} by K^+/Cu^{2+}, respectively; the catalyst $La_{0.9}K_{0.1}Co_{0.9}Ni_{0.1}O_{3-\delta}$ possesses the lowest activation energy of 84.02 kJ mol^{-1}.

Acknowledgements

This work is financially supported by the National Natural Science Foundation of China (No. 21076146), the Specialized Research Fund for the Doctoral Program of Higher Education of China (No. 20090032110013) and the Program of New Century Excellent Talents in University of China (No. NCET-07-0599). The authors are also grateful to the Program of Introducing Talents of Discipline to University of China (No. B06006).

References

[1] M.P. Walsh, SAE Paper 2001, 010183.
[2] D.H. Campbell-Lendrum, C.F. Corvalán, A. Prüss-Ustün, World Health Organization: Geneva 2003, pp. 133–158.
[3] K. Yoshida, S. Makino, S. Sumiya, G. Muramatsu, R. Helferich, SAE Paper 1989, 892046.
[4] Q. Li, M. Meng, N. Tsubaki, X.G. Li, Z.Q. Li, Y.N. Xie, T.D. Hu, J. Zhang, Appl. Catal. B 91 (2009) 406–415.
[5] N. Nejar, M.J. Illán-Gómez, Appl. Catal. B 70 (2007) 261–268.
[6] D. Reichert, H. Bockhorn, S. Kureti, Appl. Catal. B 80 (2008) 248–259.
[7] L. Castoldi, R. Matarrese, L. Lietti, P. Forzatti, Appl. Catal. B 64 (2006) 25–34.
[8] R. Matarrese, L. Castoldi, L. Lietti, P. Forzatti, Top. Catal. 52 (2009) 2041–2046.
[9] D. Fino, N. Russo, G. Saracco, V. Specchia, J. Catal. 242 (2006) 38–47.
[10] W.F. Shangguan, Y. Teraoka, S. Kagawa, Appl. Catal. B 16 (1998) 149–154.
[11] Y. Teraoka, K. Nakano, S. Kagawa, W.F. Shangguan, Appl. Catal. B 5 (1995) L181–L185.
[12] Y. Teraoka, K. Nakano, W.F. Shangguan, S. Kagawa, Catal. Today 27 (1996) 107–113.
[13] Z.Q. Li, M. Meng, Q. Li, Y.N. Xie, T.D. Hu, J. Zhang, Chem. Eng. J. 164 (2010) 98–105.
[14] Z.Q. Li, M. Meng, F.F. Dai, T.D. Hu, Y.N. Xie, J. Zhang, Fuel 93 (2012) 606–610.
[15] T. Seyama, Catal. Rev. 34 (1992) 281–300.
[16] N. Yamazoe, Y. Teraoka, Catal. Today 8 (1990) 175–199.
[17] J. Liu, Z. Zhao, C.M. Xu, A.J. Duan, G.Y. Jiang, J. Phys. Chem. C 112 (2008) 5930–5941.
[18] D. Fino, N. Russo, G. Saracco, V. Specchia, J. Catal. 217 (2003) 367–375.
[19] X.S. Peng, H. Lin, W.F. Shangguan, Z. Huang, Catal. Commun. 8 (2007) 157–161.
[20] X.S. Peng, H. Lin, W.F. Shangguan, Z. Huang, Ind. Eng. Chem. Res. 45 (2006) 8822–8828.
[21] Y. Teraoka, K. Nakano, S. Kagawa, Appl. Catal. B 34 (2001) 73–78.
[22] S.S. Hong, G.D. Lee, Catal. Today 63 (2000) 239–404.
[23] J. Oi-Uchisawa, A. Obuchi, R. Enomoto, J. Xu, T. Nanba, S. Liu, S. Kushiyama, Appl. Catal. B 32 (2001) 257–268.
[24] J. Oi-Uchisawa, A. Obuchi, S.D. Wang, T. Nanba, A. Ohi, Appl. Catal. B 43 (2003) 117–129.
[25] X.X. He, M. Meng, J.J. He, Z.Q. Zou, X.G. Li, Z.Q. Li, Z. Jiang, Catal. Commun. 12 (2010) 165–168.
[26] R.D. Shannon, Acta Crystallogr. A32 (1976) 751–767.
[27] T. Ozawa, J. Thermal Anal. Calorim. 2 (1970) 301–324.
[28] T. Ozawa, J. Thermal Anal. Calorim. 7 (1975) 601–617.
[29] O. Haas, R.P.W.J. Struis, J.M. McBreen, J. Solid State Chem. 177 (2004) 1000–1010.
[30] K.B. Li, X.J. Li, K.G. Zhu, J.S. Zhu, Y.H. Zhang, J. Appl. Phys. 81 (1997) 6943–6947.
[31] N.A. Merino, B.P. Barbero, P. Grange, L.E. Cadús, J. Catal. 231 (2005) 232–244.
[32] H. Wang, Z. Zhao, P. Liang, C.M. Xu, A.J. Duan, G.Y. Jiang, J. Xu, J. Liu, Catal. Lett. 124 (2008) 91–99.
[33] M. Kostoglou, P. Housiada, A.G. Konstandopoulos, Chem. Eng. Sci. 58 (2003) 3273–3283.

[34] J. Liu, Z. Zhao, C.M. Xu, A.J. Duan, Appl. Catal. B 78 (2008) 61–72.
[35] L. Wachowski, S. Zielinski, A. Burewixz, Acta Chim. Acad. Sci. Hung. 106 (1981) 217–242.
[36] M. Engelmann-Pirez, P. Granger, Catal. Today 107–108 (1990) 315–322.
[37] Y. Wen, C. Zhang, H. He, Y. Yu, Y. Teraoka, Catal. Today 126 (2007) 400–405.
[38] Y.G. Wang, J.W. Ren, Y.Q. Wang, F.Y. Zhang, X.H. Liu, Y. Guo, G.Z. Lu, J. Phys. Chem. C 112 (2008) 15293–15298.
[39] J.F. Moudler, W.F. Sticle, P.E. Sobol, K.D. Bomben, in: J. Chastain (Ed.), Handbook of XPS, Perkin-Elmer, Eden Prairie, MN, 1992, p. 219.
[40] R.Q. Tan, Y.F. Zhu, Appl. Catal. B 58 (2005) 61–68.
[41] Z. Zhao, X. Yang, Y. Wu, Appl. Catal. B 8 (1996) 281–297.
[42] Y. Wu, T. Wu, B.S. Dou, C.X. Wang, X.F. Xie, Z.L. Yu, S.R. Fan, Z.R. Fan, L.C. Wang, J. Catal. 120 (1989) 88–107.
[43] J.V. Craenenbroeck, D. Andreeva, T. Tabakova, K.V. Werde, J. Mullens, F. Verpoort, J. Catal. 209 (2002) 515–527.
[44] P.A.J. Neeft, M. Makkee, J.A. Moulijn, Appl. Catal. B 8 (1996) 57–78.
[45] A. Carrascull, I.D. Lick, N.P. Esther, M.I. Ponzi, Catal. Commun. 4 (2003) 124–128.
[46] S. Liu, A. Obuchi, J. Oi-Uchisawa, T. Nanba, S. Kushiyama, Appl. Catal. B 37 (2002) 309–319.
[47] J.Y. Luo, M. Meng, Y.Q. Zha, Y.N. Xie, T.D. Hu, J. Zhang, T. Liu, Appl. Catal. B 78 (2008) 38–52.
[48] J.Y. Luo, M. Meng, X.G. Li, Y.Q. Zha, Micropor. Mesopor. Mater. 113 (2008) 277–285.
[49] W.S. Epling, L.E. Campbell, A. Yezerets, N.W. Currier, J.E. Parks, Catal. Rev. 46 (2004) 163–245.
[50] S. Roy, A. Baiker, Chem. Rev. 109 (2009) 4054–4091.
[51] C. Sedlmair, K. Seshan, A. Jentys, J.A. Lercher, J. Catal. 214 (2003) 308–316.
[52] Q. Li, M. Meng, H. Xian, N. Tsubaki, X.G. Li, Y.N. Xie, T.D. Hu, J. Zhang, Environ. Sci. Technol. 44 (2010) 4747–4752.